

Path extraction in 3D medical images for virtual endoscopy

T. Deschamps

Professional Imaging System Group, LEP,

22, avenue Descartes, BP 15, F-94453 Limeil-Brévannes Cedex, France

Telephone : 33-1-45 10 68 56 Fax : 33-1-44 05 69 59

Email : deschamps@lep-philips.fr

L.D. Cohen

CEREMADE UMR CNRS 7534, Université Paris IX Dauphine,

Place du Marechal de Lattre de Tassigny, 75775 Paris Cedex 16, France

Telephone : 33-1-44 05 46 78 Fax : 33-1-44 05 45 99

Email : cohen@ceremade.dauphine.fr

January 7, 2000

Abstract

This paper presents a fast and efficient algorithm that computes a path useful for guiding endoscopic viewing that only depends on a start and end point.

This is based on previous work (Cohen and Kimmel, 1997) for extracting paths in 2D images, given only the two extremities of the path and the image as inputs, with a front propagation equation. This technique maps the active contours (Kass *et al.*, 1988) into a minimal path problem minimizing only the potential P term. It makes global minimization, reduces user interaction, and the front propagation is solved using Fast Marching (Sethian, 1996). Our original contribution is to extend this technique to 3D. We also introduce a method to extract a centered path in tubular structures, which is very useful for object with complex topology.

This work finds its motivation in the particular case of 3D medical images. We show that this technique can be efficiently applied to the problem of finding a path in tubular anatomical structures with minimum interactivity, and we apply it to virtual endoscopy. Usually path construction is left to the user who must guide by hand the virtual endoscope. But for a complex structure, the path construction in 3D images becomes a very tedious task. Using our 3D front propagation method, we propose a more automatic path tracking method to overcome those drawbacks: we are able to build a path, given only one or two endpoints. Synthetic and real medical images are used to illustrate each contribution. Virtual endoscopy results are shown for various anatomical regions (colon, brain vessels, ...) with different 3D imaging protocols (CT, MR) and different definitions of the Potential P to minimize.

keywords : Endoscopy, Virtual Reality, Medical Image Understanding, Deformable Models, Multimodal Image Segmentation.

1 Introduction

The main motivation of this work is that it enables almost automatic path tracking routine in 3D medical images for virtual endoscopy inside an anatomical object from a CT or MR image. The virtual endoscopy process consists in rendering perspective views of the inside of tubular structures of human anatomy along a user-defined path. Clinicians are then provided with an alternative to the uncomfortable and invasive diagnostic procedures of real endoscopy. Usually, the examination of a patient pathology would require threading a camera inside his body. This new method skips the camera and can give views of region of the body difficult or impossible to reach physically (e.g. brain vessels), the only requirement being X-ray exposure for CT and sometimes to inject a contrast product (dye or air) in the anatomical objects, for better detection. A major drawback in general remains when the user must define all path points manually. For a complex structure (small vessels, colon,...) the required interactivity can be very tedious. If the path is not correctly build, it can cross an anatomical wall during the virtual fly-through. Path construction is thus a very critical task and precise anatomical knowledge of the structure is needed to a set a suitable trajectory. Our work focuses on the automation of the path construction, reducing interactions and improving performance, in a robust way, given only one or two end points and the image as inputs.

With classical deformable models (Kass *et al.*, 1988), extracting a path between two fixed extremities is the solution of the minimization of an energy composed of internal and external constraints on this path, needing a precise initialization. Similarly, defining a cost function as an image constraint only, the minimal path becomes the path for which the integral of the cost between the two end points is minimal. Simplifying the model to external forces only, (Cohen and Kimmel, 1997) solved this minimal path problem in 2D with a front propagation equation between the two fixed end points, using the *Eikonal* equation (that physically models wavelight propagation), with a given initial front. Therefore, the first step is to build an image-based measure P that defines the minimality property in the studied image, and to introduce it in the *Eikonal* equation. The second step is to propagate the front on the entire image domain, starting from an initial front restricted to one of the fixed points. The propagation is done using an algorithm called *Fast Marching* developed in (Sethian, 1996).

The original contribution of our work is to adapt to 3D images the minimal path technique developed in (Cohen and Kimmel, 1997). Other improvements concerning the reduction of the computing cost and the user interactivity can be found in (Deschamps and Cohen, 2000). For the particular case of tubular anatomical structures, we also introduce a method to extract a centered path in the object of interest. We show that the Fast Marching method can be efficiently applied to the problem of finding a path in virtual endoscopy with minimum interactivity. A wide range of application areas are envisaged from colon to brain vessels. We also propose a range of choices for finding the right input potential P to the minimal path tracking.

In section 2, we summarize the method detailed in (Cohen and Kimmel, 1997) and extend it to 3D. In section 3, we explain how to extract centered paths in tubular structures. And in section 4, we apply our method to virtual endoscopy.

2 3D minimal path extraction

We are interested in this paper in finding a 3D curve for virtual endoscopy. Our approach is to extend to 3D the basic ideas of the method introduced by (Cohen and Kimmel, 1997) to find the global minimum of the active contour energy using minimal paths.

2.1 The Cohen-Kimmel Method

The energy to minimize is similar to classical deformable models (see (Kass *et al.*, 1988)) where it combines smoothing terms and image features attraction term (Potential P):

$$E(C) = \int_{\Omega} \left\{ w_1 \|C'(s)\|^2 + w_2 \|C''(s)\|^2 + P(C(s)) \right\} ds \quad (1)$$

where $C(s)$ represents a curve drawn on an image, Ω is its domain of definition $[0, L]$, and L is the length of the curve. It reduces the user initialization to giving the two end points of the contour C . In (Cohen and Kimmel, 1997), the authors have related this problem with the new paradigm of the level-set formulation. In particular, its Euler equation is equivalent to the geodesic active contours (Caselles *et al.*, 1995). They introduced a model which improves energy minimization because the problem is transformed in a way to find the global minimum. It avoids the solution being stucked in local minima. Let us explain each step of this method.

Most of the classical deformable contours have no constraint on the parameterization s , thus allowing different parameterization of the contour C to lead to different results. In (Cohen and Kimmel, 1997), contrary to the classical snake model (but similarly to geodesic active contours), s represents the arc-length parameter. This means that $\|C'(s)\| = 1$, and considering a simplified energy model without a second derivative term leads to the formulation

$$E(C) = \int_{\Omega} \{w + P(C(s))\} ds \quad (2)$$

We now have an expression in which the internal forces are included in the external potential. The regularization of this model is now achieved by the constant $w > 0$. This term integrates as $\int_{\Omega} w ds = w \times \text{length}(C)$ and allows us to control the smoothness of the contour (see (Cohen and Kimmel, 1997) for details).

Given a potential $P > 0$ that takes lower values near desired features, we are looking for paths along which the integral of $\tilde{P} = P + w$ is minimal. We can define the surface of minimal action U , as the minimal energy integrated along a path between a starting point p_0 and any point p :

$$U(p) = \inf_{\mathcal{A}_{p_0,p}} E(C) = \inf_{\mathcal{A}_{p_0,p}} \left\{ \int_{\Omega} \tilde{P}(C(s)) ds \right\} \quad (3)$$

where $\mathcal{A}_{p_0,p}$ is the set of all 3D paths between p_0 and p . The minimal path between p_0 and any point p_1 in the image can be easily deduced from this action map. Assuming that potential P is always positive, the action map will have only one local minimum which is the starting point p_0 , and the minimal path will be found by a simple back-propagation on the energy map. Thus, contour initialization is reduced to the selection of the two extremities of the path.

2.2 3D Fast-Marching resolution

In order to compute this map U , a front-propagation equation related to equation (3) is solved : $\frac{\partial C}{\partial t} = \frac{1}{\tilde{P}} \vec{n}$. It evolves a front starting from an infinitesimal circle shape around p_0 until each point inside the image domain is assigned a value for U . The value of $U(p)$ is the time t at which the front passes over the point p . Then it notifies the shortest path energy to reach the start point from any point in the image.

The fast marching technique, introduced by (Sethian, 1996), was used by (Cohen and Kimmel, 1997) noticing that the map U satisfies the Eikonal equation:

$$\|\nabla U\| = \tilde{P} \quad (4)$$

Classic finite difference schemes for this equation tend to overshoot and are unstable. (Sethian, 1996) has proposed a method which relies on a one-sided derivative that looks in the up-wind direction of the moving front, and thereby avoids the over-shooting associated with finite differences. The 2D scheme equation developed in (Rouy and Tourin, 1992) is extended to 3D, leading to the scheme

$$\begin{aligned} & (\max\{u - U_{i-1,j,k}, u - U_{i+1,j,k}, 0\})^2 + \\ & (\max\{u - U_{i,j-1,k}, u - U_{i,j+1,k}, 0\})^2 + \\ & (\max\{u - U_{i,j,k-1}, u - U_{i,j,k+1}, 0\})^2 = \tilde{P}_{i,j,k}^2 \end{aligned} \quad (5)$$

giving the correct viscosity-solution u for $U_{i,j,k}$. The complete resolution of this scheme is detailed in (Deschamps and Cohen, 2000), where we extend the *fast marching* method, introduced by (Sethian, 1996) and used by (Cohen and Kimmel, 1997) to our 3D problem.

The improvement made by the *fast marching* is to introduce order in the selection of the grid points. This order is based on the fact that information is propagating *outward*, because action can only grow due to the quadratic equation (5). The *fast marching* technique select at each iteration the *Trial* point with minimum action value. This technique of considering at each step only the necessary set of grid points was originally introduced for the construction of minimum length paths in a graph between two given nodes in (Dijkstra, 1959). Thus it needs only one pass over the image. To perform efficiently these operations in minimum time, the *Trial* points are stored in a min-heap data structure (see details in (Sethian, 1996)). Since the complexity of the operation of changing the value of one element of the heap is bounded by a worst-case bottom-to-top proceeding of the tree in $O(\log_2 N)$, the total work is about $O(N \log_2 N)$ for the *fast marching* on a N points grid.

Therefore, finding the shortest path between any point p and the starting point p_0 is simply done by back-propagation on the computed minimal action map, until p_0 is reached, p_0 being its global minimum.

2.3 Example of a minimal path extraction

The minimal action map U computed according to the discretization scheme of equation (3) is similar to convex, in the sense that its only local minimum is the global minimum found at the front propagation start point p_0 where $U(p_0) = 0$. The gradient of U is orthogonal to the propagating fronts since these are its level sets. Therefore, the minimal action path between any point p and the start point p_0 is found by sliding back the map U until it converges to p_0 . It can be done with a simple steepest gradient descent, with a predefined descent step, on the minimal action map U , choosing $p_{n+1} = p_n - \text{step} \times \nabla U(p_n)$. See in figure 1-middle the action map corresponding to a binarized potential defined by high values in a spiral rendered in figure 1-middle. The path found between a point in the center of the spiral and another point outside is shown in figure 1-right by transparency. Several important issues concerning the back-propagation technique are detailed in (Deschamps and Cohen, 2000), where we show how to constrain the computations to a small subset of the images.

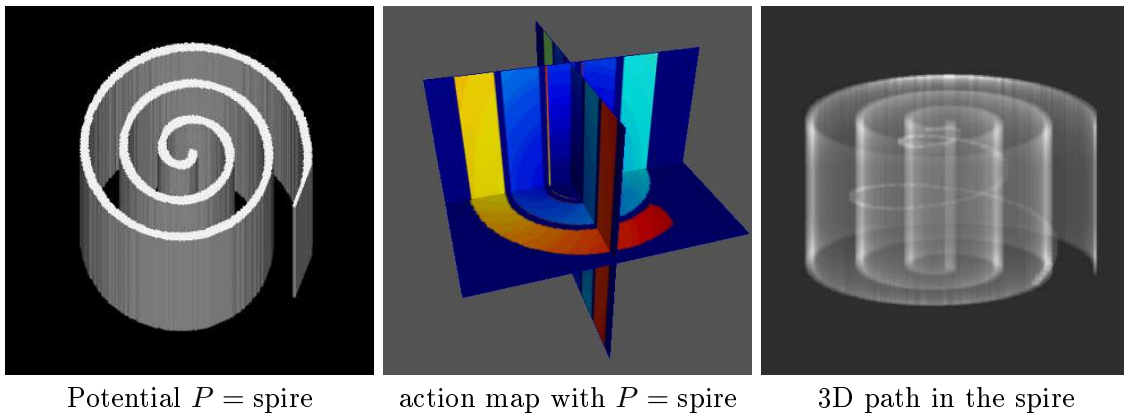


Figure 1: Examples on synthetic potentials

3 The path centering method

In this section we derive a technique to track paths that are centered in a tubular shape, using the front propagation methods. To illustrate this problem, we use example shown on figure 2-left, which is a binarized image of brain vessels. Using our classical front propagation, the minimal path extracted is tangential to the edges, as shown in figure 2-middle, superimposed on the action map computed. This is due to the fact that length is minimized. This path is not tuned for problems which may require a centered path, like virtual endoscopy.

In some cases it is possible to get the shape of the object in which we are looking for a path. One way of making this shape available is to use the front propagation itself as shown in Figure 5. This is more detailed in (Deschamps and Cohen, 2000). If we have the shape of our object, we can use a front propagation method to compute the distance to its edges using a potential defined by

$$\begin{aligned}
 P(i, j) &= 1 & \forall (i, j) \in \{object\} \\
 P(i, j) &= \infty & \forall (i, j) \in \{Background\} \\
 P(i, j) &= 0 & \forall (i, j) \in \{Interface\}
 \end{aligned}$$

When this distance map, noted \mathcal{E} , is computed, it is used to create a potential P' which weights the points in order to propagate faster a new front in the centre of the desired regions. Choosing a value d to be the minimum acceptable distance to the walls, we propose the following potential:

$$P'(\mathbf{x}) = \{|d - \min(\mathcal{E}(\mathbf{x}); d)|\}^\gamma \quad (6)$$

According to this new penalty, the final front propagates faster in the center of the vessel. This can be observed by looking at the shape of the iso-action lines of the centered minimal action shown in figure 2-right. Finally, the path avoids the edges and remains in the center of the vessel, while the former path tangential to edges. Results on real 3D data are shown in section 4.

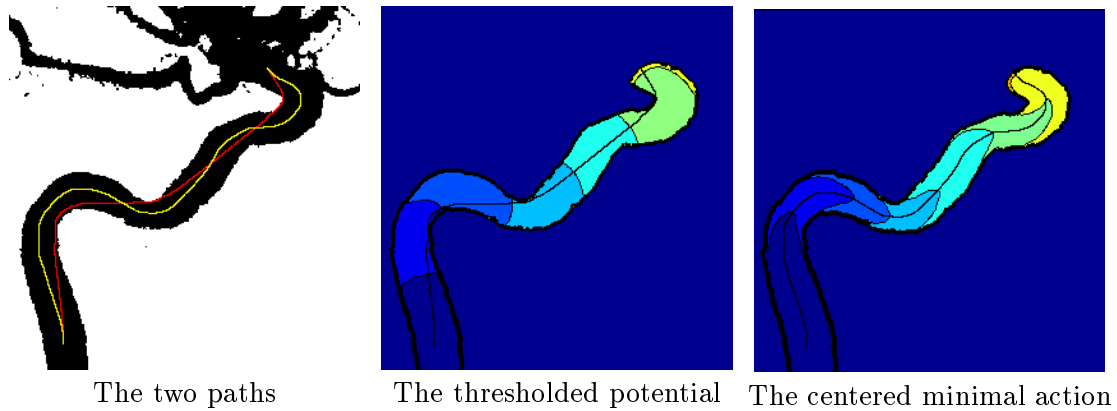


Figure 2: Comparing classic and centered paths

4 Application to Virtual Endoscopy

Visualization of volumetric medical image data plays a crucial part for diagnosis and therapy planning. The better the anatomy and the pathology are understood, the more efficiently one can operate with low risk. Different possibilities exist for visualizing 3D data: three 2D orthogonal views (see figure 3), maximum intensity projection (MIP, and its variants, see figure 10), surface and volume rendering. In particular, virtual endoscopy

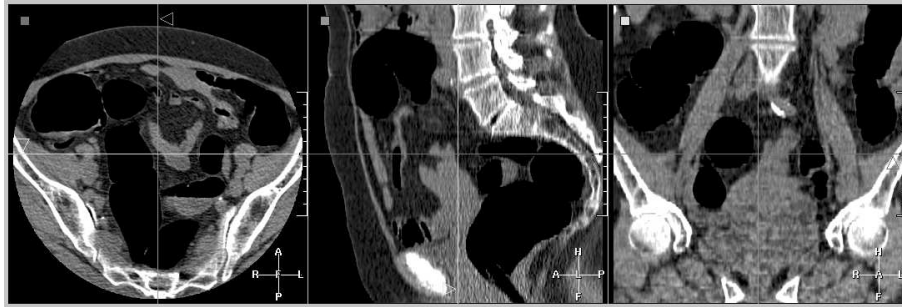


Figure 3: Three orthogonal views of a volumetric CT data set of the Colon

allows by means of surface/volume rendering techniques to visually inspect regions of the body that are dangerous and/or impossible to reach physically with a camera. A virtual endoscopic system is usually composed of two parts:

1. A Path construction part, which provides the successive locations of the fly-through the tubular structure of interest (see figure 4-left);
2. Three dimensional viewing along the endoscopic path (see figure 4-right).

A major drawback in general remains when the path construction is left to the user who manually has to “guide” the virtual endoscope/camera. The required interactivity on a 3D image can be very tedious for complex structures such as the Colon.

Since the anatomical objects have often complex topologies, the path passes in and out of the three orthogonal planes. Consequently the right location is accomplished by alternatively entering the projection of the wanted point in each of the three planes. Then, the

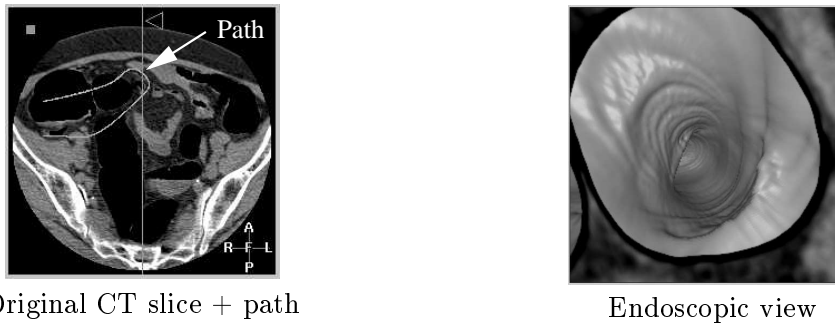


Figure 4: Interior view of a Colon, reconstructed from a defined path

path is approximated between the user defined points by lines or Bezier splines, and if the number of points is not enough, it can easily cross an anatomical wall. Path construction in 3D images is thus a very critical task and precise anatomical knowledge of the structure is needed to set a suitable trajectory, with the minimum required interactivity.

The front propagation techniques studied in this paper, propose an alternative to this tedious path construction by building paths in 3D images with minimum interactivity. We first apply this method to the case of virtual endoscopy in a Colon CT dataset, then we extend this technique to other anatomical objects.

Application to Colonoscopy

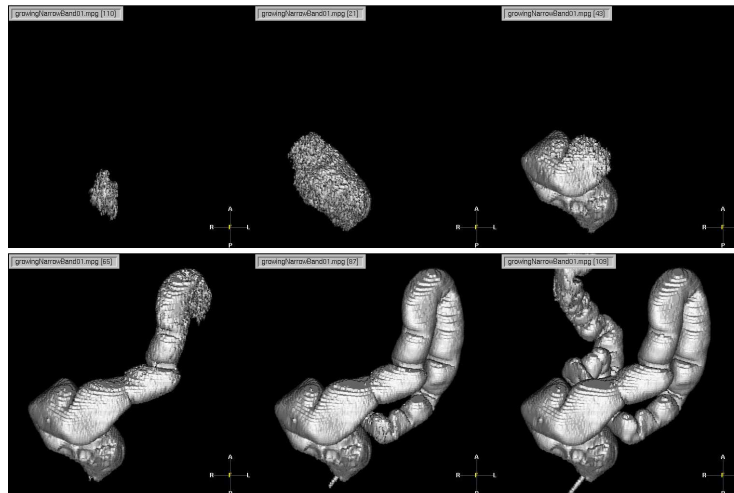


Figure 5: Successive steps of front propagation inside the Colon volume

All tests are performed on a volumetric CT scan of size $512 \times 512 \times 140$ voxels, shown in figure 3. We define a potential P from the 3D image $I(x)$ that is minimal inside the anatomical shapes where end points are located. We chose the potential $P(x) = |I(x) - I_{mean}|^\alpha + w$, where an average grey level value I_{mean} of the Colon is obtained with an histogram. From this definition, P is lower inside the Colon in order to propagate the front faster. Also, edges are enhanced with a non-linear function ($\alpha > 1$) since the path to be extracted is in a large object that have complex shape and very thin edges. Then,

using this potential, we propagate inside the Colon creating a path between a couple of given points. In fact, the Colon being a closed object with two extremities, this allows to give only one end point for front propagation. This method is explained in (Deschamps and Cohen, 2000). The figure 5 shows the result of the fast marching technique with a unique starting point belonging to the Colon and an Euclidean path length criterion of 500 mm.

However, this potential does not produce paths relevant for virtual endoscopy. Indeed,

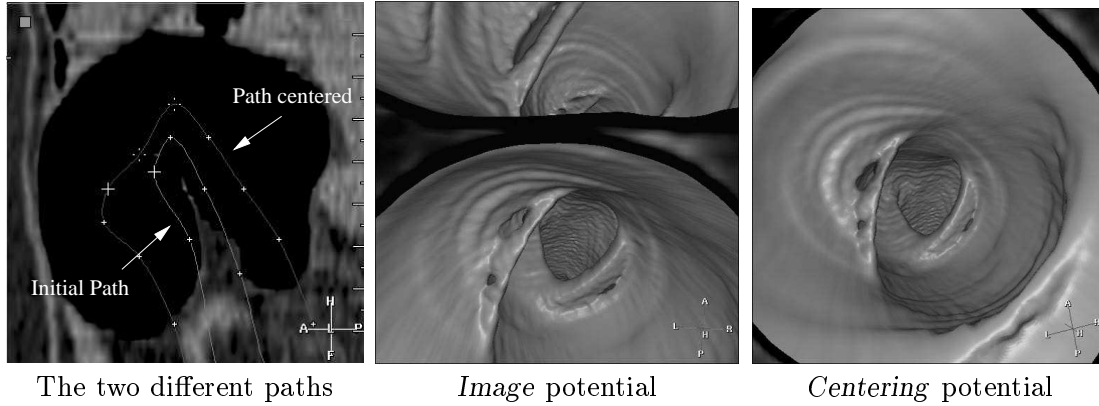


Figure 6: Centering the path in the Colon.

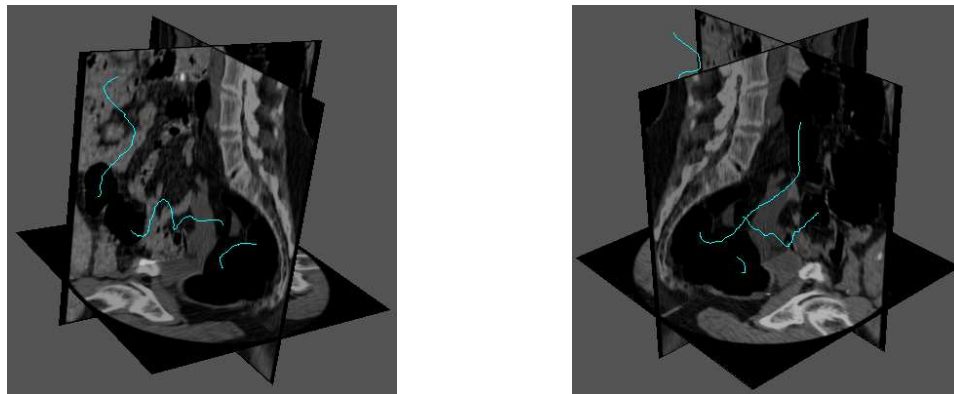


Figure 7: 3D views of a path inside the Colon.

paths should remain not only in the anatomical object of interest but as far as possible from its edges. In order to achieve this target, we use the centering potential method as detailed in section 3. This approach needs a *shape* information. This information is provided by the previous front propagation. From its definition, the front sticks to the anatomical shapes as shown in figure 5. This is related to the use of Fast Marching algorithm to extract a surface for segmentation (Malladi and Sethian, 1998). It gives a rough segmentation of the Colon and provides a good information and a fast-reinitialization technique to compute the distance to the edges. Using this thresholded map as a potential that indicates the distance to the walls, we can correct the initial path as shown in figure 6-left. Both 3D paths are projected on the 2D slice for visualization. As expected, the new path remains more in the middle of the Colon. The two different cross-sections in figures 6-middle and 6-right display the view of the interior of the Colon from both paths at the u-turn shown in figure 6-left. This effect of centering the path enhances dramatically the rendering of

the video sequence of virtual endoscopy obtained.¹ With the initial potential, the path is near the wall, and we see the u-turn, whereas with the new path, the view is centered into the Colon, giving a more correct view of the inside of the Colon.

Therefore, the two end points can be connected correctly, giving a path staying inside the anatomical object. The results are displayed in two 3D views in figure 7. But for virtual Colonoscopy, it is often not necessary to set the two end points within the anatomical object.

Application to a Trachea CT scan

Extracting paths inside the Trachea (see figure 8) is the same problem than in the Colon. Air fills the object and give a shape information all along from mouth to lungs. Therefore,



Figure 8: A slice of the 3D dataset of the Trachea and an endoscopic view inside it.

the anatomical object having a very simple topology, the path construction with one or two fixed points is easier than in the Colon case. One example path tracks the Trachea, using a nonlinear function of the image grey levels ($P(x) = |I(x) - 200|^2 + 1$). An endoscopic view along the path is displayed in figure 8-right, and two views of this path are shown in figure 9.



Figure 9: 3D views of a path inside the Trachea.

¹This video will be shown at a presentation, and could be made available for reviewers on a web site if required.

Application to a Brain MRA image

Tests were performed on Brain vessels in a magnetic resonance angiography (MRA) scan (a maximum-intensity-projection (MIP) view of the Brain vessels is shown in figure 10). The problem is different, because there is only signal from blood. All other structures have been removed. The main difficulty here lies in the variations of the dye intensity. The path shown from two viewpoints tracks (see figure 11) the superior sagittal venous canal, using a nonlinear function of the image dye intensity ($P(x) = |I(x) - 100|^2 + 1$). An endoscopic

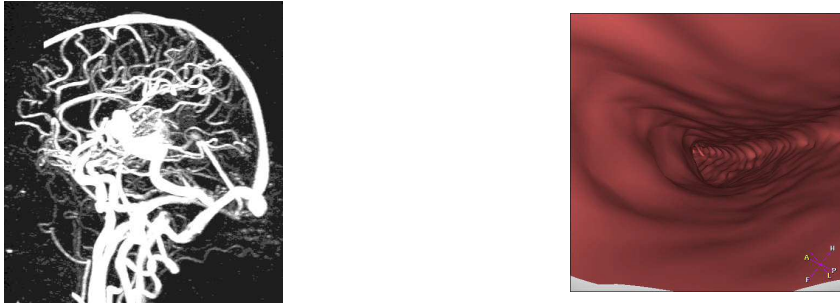


Figure 10: MIP and endoscopic views of Brain vessels in a MRA volume.

view along this path is shown in figure 10-right.

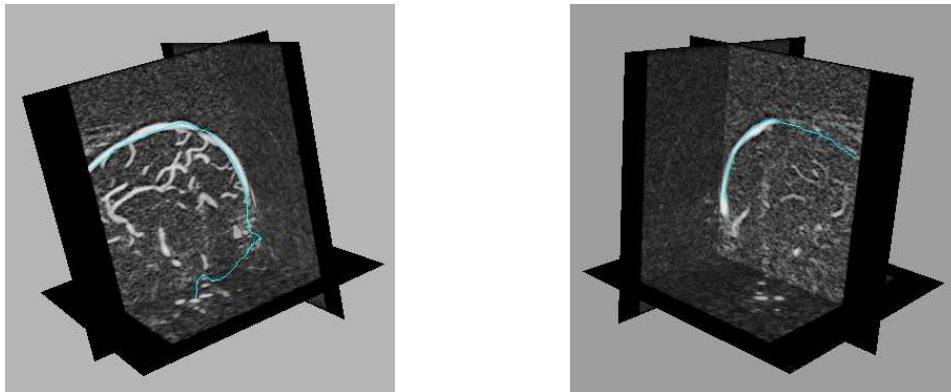


Figure 11: 3D views of a path inside the Brain Vessels.

Application to an Aorta MR scan

A test was made on an Aorta dataset in a MR scan shown in figure 12-left. The propagation potential is based on a nonlinear function of the intensity of the contrast solution that fills the Aorta. Tracking the Aorta in this dataset is difficult since the intensity of the contrast product will vary along the Aorta (the contrast bolus dilutes during the acquisition time). This non-uniformity could make a path cross other anatomical structures with similar intensities. One example path tracks one iliaca, using the potential $P(x) = |I(x) - 1000|^2 + 1$ in the MRcan. We have displayed an endoscopic view along this path in figure 12-right. We have displayed an endoscopic view along the path in figure 12-right.



Figure 12: A slice of the 3D Aorta MR dataset and an endoscopic view inside it.

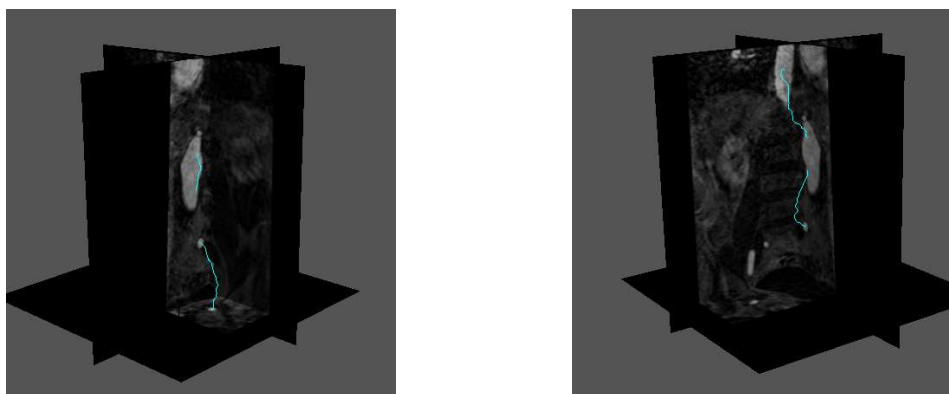


Figure 13: 3D views of a path inside the Aorta.

5 Conclusion

In this paper we presented a fast and efficient algorithm that computes a path useful for guiding endoscopic viewing that only depends on a start and end point.

This work was the extension to 3D of a level-set technique developed in (Cohen and Kimmel, 1997) for extracting paths in 2D images, given only the two extremities of the path and the image as inputs, with a front propagation equation. This technique improves energy minimization, reduces user interaction, of the classical deformable models, and is solved using a very fast numerical implementation developed by (Sethian, 1996).

We showed that this technique can be efficiently applied to the problem of finding a path in tubular anatomical structures for virtual endoscopy with minimum interactivity, and we developed a method to extract centered paths in tubular anatomical structures. The results were promising for several clinical applications, including those with very complex topology. In particular we extracted centered paths inside a CT dataset of the colon, and in a MR datasets of the brain vessels. We have proved the benefit of our method towards classical virtual endoscopy: examination of a patient pathology no more requires threading a camera inside his body, and only a few seconds are necessary to build a complete trajectory inside the body, giving only one or two end points and the image as inputs.

References

- Caselles, V., Kimmel, R., and Sapiro, G. (1995). Geodesic active contours. In *ICCV'95*, pp. 694–699, Cambridge, USA.
- Cohen, L.D. and Kimmel, R. (1997). Global minimum for active contour models: A minimal path approach. *International Journal of Computer Vision*, 24(1), 57–78.

- Deschamps, T. and Cohen, L.D. (2000). Minimal path in 3d images and application to virtual endoscopy. Technical report, Laboratoire Cérémade, Université Paris Dauphine.
- Dijkstra, E.W. (1959). A note on two problems in connection with graphs. *Numerische Mathematic*, 1, 269–271.
- Kass, M., Witkin, A., and Terzopoulos, D. (1988). Snakes: Active contour models. *International Journal of Computer Vision*, 1(4), 321–331.
- Malladi, R. and Sethian, J.A. (1998). A real-time algorithm for medical shape recovery. In *Proceedings of International Conference on Computer Vision*, pp. 304–310.
- Rouy, E. and Tourin, A. (1992). A viscosity solution approach to shape-from-shading. *SIAM Journal of Numerical Analysis*, 29, 867–884.
- Sethian, J.A. (1996). *Level set methods: Evolving Interfaces in Geometry, Fluid Mechanics, Computer Vision and Materials Sciences*. Cambridge University Press, University of California, Berkeley.